Flexibility of Ras Lipid Modifications Studied by ^{2}H Solid-State NMR and Molecular Dynamics Simulations

Alexander Vogel,* Kui-Thong Tan,[†‡] Herbert Waldmann,[†‡] Scott E. Feller,[§] Michael F. Brown,[¶] and Daniel Huster*

*Junior Research Group "Structural Biology of Membrane Proteins", Institute of Biotechnology, Martin Luther University Halle-Wittenberg, Halle, Germany; [†]Max Planck Institute of Molecular Physiology, Dortmund, Germany; [‡]University of Dortmund, Department of Chemical Biology, Dortmund, Germany; [§]Department of Chemistry, Wabash College, Crawfordsville, Indiana; and [¶]Departments of Chemistry and Physics, University of Arizona, Tucson, Arizona

ABSTRACT Human posttranslationally modified N-ras oncogenes are known to be implicated in numerous human cancers. Here, we applied a combination of experimental and computational techniques to determine structural and dynamical details of the lipid chain modifications of an N-ras heptapeptide in 1,2-dimyristoyl-*sn*-glycero-3-phosphocholine (DMPC) membranes. Experimentally, ^{2}H NMR spectroscopy was used to study oriented membranes that incorporated ras heptapeptides with two covalently attached perdeuterated hexadecyl chains. Atomistic molecular dynamics simulations of the same system were carried out over 100 ns including 60 DMPC and 4 ras molecules. Several structural and dynamical experimental parameters could be directly compared to the simulation. Experimental and simulated ^{2}H NMR order parameters for the methylene groups of the ras lipid chains exhibited a systematic difference attributable to the absence of collective motions in the simulation and to geometrical effects. In contrast, experimental ^{2}H NMR spin-lattice relaxation rates for Zeeman order were well reproduced in the simulation. The lack of slower collective motions in the simulation did not appreciably influence the relaxation rates at a Larmor frequency of 115.1 MHz. The experimental angular dependence of the ^{2}H NMR relaxation rates with respect to the external magnetic field was also relatively well simulated. These relaxation rates showed a weak angular dependence, suggesting that the lipid modifications of ras are very flexible and highly mobile in agreement with the low order parameters. To quantify these results, the angular dependence of the ^{2}H relaxation rates was calculated by an analytical model considering both molecular and collective motions. Peptide dynamics in the membrane could be modeled by an anisotropic diffusion tensor with principal values of $D_{\|} = 2.1 \times 10^9\,s^{-1}$ and $D_{\perp} = 4.5 \times 10^5\,s^{-1}$. A viscoelastic fitting parameter describing the membrane elasticity, viscosity, and temperature was found to be relatively similar for the ras peptide and the DMPC host matrix. Large motional amplitudes and relatively short correlation times facilitate mixing and dispersal with the lipid bilayer matrix, with implications for the role of the full-length ras protein in signal transduction and oncogenesis.

INTRODUCTION

Posttranslational lipid modifications play a key role in the membrane association of 5–10% of all cellular membrane proteins (1,2). Lipid modification mainly serves as a membrane anchoring mechanism, but is also discussed as a mediator in protein-protein interactions (3). An interesting structural variety of lipid modifications such as GPI anchors, geranylgeranylated, or farnesylated/palmitoylated proteins has evolved (2). In addition to multipally lipidated proteins, single lipid modifications are common in amplifying and directing the interaction between basic protein segments and negatively charged membrane domains. For membrane association by lipid modification in combination with electrostatic interactions, N-myristoylation or S-farnesylation appears to be the most prevalent structural motifs. Ras proteins are very important examples of lipid modified proteins, as they are mediators in an important biological signal transduction cascade. Ras is a GTP binding protein that regulates cell proliferation and differentiation (4). Three isoforms with different posttranslational modifications exist. They can be distinguished by the number of lipid chains as they acquire one (K-ras), two (N-ras), or three (H-ras) lipid posttranslational modifications. If ras is mutated, uncontrolled cell growth and cancer can occur, as found in ~30% of all human cancers (4). The N-ras isoform comprises 186 amino acids and is farnesylated at Cys-186 and palmitoylated at Cys-181 (5).

Despite the structural diversity of these membrane anchors, evidently a single lipid modification is insufficient to stably attach a protein to a lipid membrane (6,7). From physicochemical considerations, partitioning of a fatty acid into a membrane is highly energetically favorable. Each methylene segment of a hydrocarbon chain that partitions into a membrane contributes −3.45 kJ/mol to the binding energy (7–10). For a single acyl chain, a unitary Gibbs free energy for partitioning into *n*-heptane of $\Delta G^{O} = (17.81 - 3.45 n_C)$ kJ/mol has been determined (8). Thus, ~−35 kJ/mol of binding energy arises from a single palmitoyl lipid chain modification. Although this value represents a significant favorable energy, entropic terms further reduce the actual binding of the lipid-modified protein. Membrane-associated proteins experience an unfavorable entropy as they lose translational and

Submitted January 16, 2007, and accepted for publication May 29, 2007.

Address reprint requests to Daniel Huster, Tel: 49-345-55-24942; E-mail: daniel.huster@biochemtech.uni-halle.de.

Editor: Peter Tieleman.

0006-3495/07/10/2697/16 $2.00

doi: 10.1529/biophysj.107.104562

rotational degrees of freedom upon binding (9). Theoretical estimates indicate that only ~20% of singly palmitoylated protein molecules would be associated with the membrane, explaining the necessity of the second lipid modification for stable membrane binding (7). In addition, the lipid membranes are in a fluid phase, which means that their acyl chains undergo rapid isomerizations, large amplitude motions, and interchange between a very large number of conformational states (11–13). Moreover, chain upturns and backfolding are frequently observed in these systems (11). These effects are due to the thermal energy of the system, and lead to a roughness of the membrane surface, with a broad lipid-water interface that occupies approximately half of the membrane thickness (14).

We have recently studied structural and dynamical aspects of N-ras peptides and proteins (15–19). Using solid-state NMR techniques, we have determined an initial structural model for the terminal seven amino acids with the lipid modifications (18). Further, the dynamical aspects of the membrane-binding C-terminal polypeptide chain of ras and its lipid modifications have been studied for the entire ras protein (19). This and other recent experimental work has suggested that the lipid modifications of proteins and peptides are even more mobile and flexible than the fatty acids of the phospholipids in the membrane (17). In this regard, solid-state ^{2}H NMR techniques are well-suited to investigate structural and dynamical aspects of acyl chains in a combined approach (13). The 16:0 lipid modification of ras shows lower ^{2}H NMR order parameters and higher spin-lattice relaxation rates than the phospholipid chains of the surrounding matrix. Taken together, these data indicate that the lipid-chain modifications of the ras peptide have the elastic properties of very soft materials, such as phospholipid chains in the presence of a detergent (17). However, thus far our analysis of the ras lipid chain mobility has been qualitative.

In this article, we use a combined experimental and computational approach to develop a more quantitative understanding of the mobility of ras. The experimental ^{2}H NMR studies involved spin-lattice relaxation rates for macroscopically oriented samples. Unlike in solution, relaxation rates in the solid state exhibit a pronounced dependence on the orientation of all tensor interactions with respect to the external magnetic field (20,21). In ^{2}H NMR, the largest element of the electric field gradient tensor is coincident with the C-^{2}H bond axis. If the membranes are macroscopically aligned, this orientational dependence can be observed experimentally by rotating the sample in the magnetic field, and acquiring relaxation rates for each desired angle. From the angular anisotropy, more detailed dynamical information is available compared to random (powder-type) samples. Because the total sample volume in oriented samples is restricted, and the filling factor of the radiofrequency coil is unfavorable, the experiments were carried out on a truncated ras heptapeptide rather than the full-length ras protein. Data were acquired for a doubly lipid modified ras heptapeptide from the N-terminus of the ras protein containing two perdeuterated hexadecyl chain modifications.

Such experimental ^{2}H NMR data can be quantitatively analyzed either in terms of simplified analytical models (22) or by atomistic molecular dynamics simulations (23); both approaches are highly complementary. In each case, models that describe the molecular motion in terms of a correlation function are introduced for analysis of the orientation-dependent ^{2}H relaxation rates. The Fourier transforms of these correlation functions—called spectral density functions—are directly proportional to the macroscopically observed relaxation rates. From the analytical models the dynamics of the molecule can be inferred. Detailed atomistic information on the molecular dynamics has been gathered from the angular anisotropy of the relaxation rates of bilayer membranes (13, 24–28). Moreover, correlation functions can be computed directly from molecular dynamics (MD) simulations, a field that has advanced remarkably in the last decade (29). As the systems studied have become larger and their trajectories longer, simulations are now at the point where experimental parameters such as electron density profiles (30), ^{2}H NMR order parameters (31,32), NMR relaxation rates (32–34), and nuclear Overhauser effects (35,36) can be reproduced with sufficient accuracy. Even large membrane proteins such as G protein-coupled receptors are now routinely simulated in an explicit membrane environment (37–40).

Here we report a combined study of experimental ^{2}H NMR order parameters and relaxation rates of a ras heptapeptide with two perdeuterated hexadecyl chain modifications. The experimental data were compared with an analytical theory, where the motions of ras are described quantitatively by an anisotropic diffusion tensor. For comparison, a MD simulation was carried out with four ras heptapeptides in a 1,2-dimyristoyl-*sn*-glycero-3-phosphocholine (DMPC) lipid matrix over 100 ns. The experimental orientation-dependent spin-lattice relaxation rates could be well reproduced by the analytical theory as well as the MD simulations. Taken together, the experimental and computational data suggest that the lipid modifications of ras are highly mobile and flexible in the liquid-crystalline membrane environment. A detailed quantitative discussion of the ras peptide mobility in comparison with literature data for phospholipids and the peptide gramicidin is provided. The flexibility of the lipidated ras-d_{66} chains provides a rationale for their membrane binding in terms of elastic deformation of the bilayer, and is relevant to the mechanism of action of the human N-ras oncogene products.

MATERIALS AND METHODS

Sample preparation

1,2-Dimyristoyl-*sn*-glycero-3-phosphocholine (DMPC) was procured from Avanti Polar Lipids (Alabaster, AL) and used without further purification. Protected amino acids and coupling reagents were obtained from Novabiochem (La Jolla, CA) and $^2H_{33}$-labeled hexadecyl alcohol from Isotec (Miamisburg, OH). The ras peptide with the amino-acid sequence H-Gly-Cys(HD-d_{33})-Met-Gly-Leu-Pro-Cys(HD-d_{33})-OMe was synthesized following Hinterding

et al. (41), Nägele et al. (42), and Schelhaas et al. (43), where HD-d_{33} indicates the perdeuterated hexadecyl thioether modifications. Aliquots of ras-d_{66} peptide and phospholipid (1:15 molar ratio) were combined in chloroform, spread onto glass plates (5 mm × 8 mm, 0.04 mg/mm^2), and slowly dried overnight at 500 mbar. The samples were hydrated for at least 24 h via the vapor phase of a saturated $CaSO_4$ solution, providing a relative humidity of 98%. The glass plates were stacked, wrapped in parafilm, transferred into a 7-mm glass tube, and sealed. The glass tube contained a reservoir of the saturated $CaSO_4$ solution that was in permanent contact with the sample to provide the identical relative humidity throughout the experiment. The sample was stored at 4°C before measurement.

Deuterium solid-state NMR spectroscopy

The ^{2}H NMR spectra were acquired with a widebore Bruker Avance750 NMR spectrometer (Rheinstetten, Germany) operating at a resonance frequency of 115.1 MHz for ^{2}H (magnetic field strength of 17.6 T). A single-channel solids probe having a 7-mm solenoid coil equipped with a goniometer was used. ^{2}H NMR spectra were accumulated for varying angles between the macroscopically oriented bilayers and the external magnetic field. Data were acquired with a spectral width of ±250 kHz using quadrature phase detection, a phase-cycled quadrupolar echo sequence (44) with two 3.5–4 μs $\pi/2$ pulses separated by a 60-μs delay, and a relaxation delay of 1 s. A phase-cycled inversion-recovery quadrupolar echo pulse sequence was used to measure the relaxation times for the decay of Zeeman order (T_{1Z}, spin-lattice relaxation time). The T_{1Z} relaxation times were measured under varying sample orientations. A relaxation delay of 2 s was used, and all other parameters were the same as for recording the ^{2}H NMR spectra. The signals were left-shifted after acquisition to initiate the Fourier transformation beginning at the top of the quadrupolar echo. Only data from the real channel were processed to yield symmetrized ^{2}H NMR spectra. An exponential line broadening not exceeding 50 Hz was applied. The ^{2}H NMR measurements were carried out at a temperature of 40°C.

From the oriented ^{2}H NMR spectra, the order parameter profiles were directly determined from the observed quadrupolar splittings ($\Delta\nu_Q$) at 0° orientation between the membrane normal and the $\boldsymbol{B_0}$ field according to

$$|\Delta\nu_Q^{(i)}| = \frac{3}{2}\chi_Q|S_{CD}^{(i)}|. \quad (1)$$

Here $\chi_Q = e^2qQ/\hbar$ represents the quadrupolar coupling constant (167 kHz for ^{2}H in an aliphatic C–^{2}H bond), and $S_{CD}^{(i)} = 1/2\langle 3\cos^2\beta_i - 1\rangle$ is the segmental order parameter. The signal doublets were assigned starting at the terminal methyl group, which exhibits the smallest quadrupolar splitting. Methylene groups were assigned consecutively according to their increasing quadrupolar splittings.

The experimental ^{2}H NMR lineshapes were simulated using 12 doublets of Lorentzian lines (labeled *a–m* in the corresponding figures). The lineshape fits were scaled in the frequency dimension by the second Legendre polynomial for the respective orientational angle of the sample. The spin-lattice relaxation times of each peak at a given sample orientation were determined from fits of inversion recovery data. All simulations and the implementation of the analytical theory below were carried out using Mathcad 2001 (MathSoft, Cambridge, MA).

Molecular dynamics simulations

Together with the experimental work, an MD simulation of ras peptides in a DMPC matrix was carried out. The calculations were performed in parallel on eight processors with a clock frequency of 2.4 GHz giving 1 ns of simulation in approximately one day. The periodic simulation cell contained 4-ras peptide molecules, 60 DMPC lipid molecules, and 1186 water molecules. The surface area was estimated from the experimentally measured deuterium order parameters and the relation between order parameters and molecular surface area (45). For the hexadecyl-d_{33} chains of the ras peptides, the previously published order parameters were used (16). The ϕ- and ψ-torsion angles for the peptide backbone were chosen arbitrarily for an approximately parallel insertion of the two lipid modifications and the hydrophobic side-chains Leu and Met into the membrane. This follows the model previously derived on the basis of ^{1}H magic-angle spinning nuclear Overhauser enhancement spectroscopy (NOESY) measurements of the ras peptide in the membrane (15,16). The program CHARMM (46) was employed for the simulation and its analysis, using the CHARMM all-H CMAP protein force field (47) with the all-H lipid force field, including a recent refinement of the saturated acyl-chain torsions (48). Initial conformations of the ras peptides were generated from a 10-ns simulation of a peptide in a membrane mimetic environment (water/hexadecane interface). Randomly sampled peptide conformations were placed into a previously equilibrated DMPC bilayer by replacing a lipid molecule, and approximately aligning the C2 carbon positions of the ras and DMPC acyl chains. The simulation was run under conditions of constant temperature (40°C), surface area, and normal pressure (1.013 bar) for 118 ns with the initial 18 ns discarded as equilibration. The smooth particle-mesh Ewald algorithm was used to compute the electrostatic forces (49). The SHAKE algorithm was used to maintain rigid all bonds involving hydrogen atoms (50), allowing a 2-fs time step.

THEORY

Angular-dependent ^{2}H relaxation rates

Random fluctuations yielding time-dependent perturbations of the Zeeman Hamiltonian lead to the relaxation of nuclear spins. In the case of ^{2}H NMR, the perturbing quadrupolar interaction depends on the orientation of the principal axes of the second-rank electric field gradient (EFG) tensor. For a detailed understanding of the measured angular-dependent ^{2}H relaxation rates, a motional model is needed, in which the stochastic fluctuations of the EFG tensor are described. The measured spin-lattice relaxation rates (R_{1Z}) are proportional to the laboratory-frame spectral density functions $J_m(\omega)$, which provide a measure for the strength of the fluctuating fields that relax the spin state:

$$R_{1Z} = \frac{3}{4}\pi^2\chi_Q^2[J_1(\omega_D, \beta_{DL}) + 4J_2(2\omega_D, \beta_{DL})]. \quad (2)$$

Here β_{DL} denotes the angle of the membrane normal of the sample with respect to the external magnetic field $\boldsymbol{B_0}$, and ω_D is the ^{2}H nuclear Larmor frequency. The spectral densities of motion are defined as the Fourier transformation of the correlation functions $G_m(t)$,

$$J_m(\omega) = \mathrm{Re}\int_{-\infty}^{\infty} G_m(t)\exp(-i\omega t)dt, \quad (3)$$

where $m = 0, \pm1, \pm2$ is the angular momentum projection index. All information about the molecular motions that lead to ^{2}H spin relaxation is contained in the second-rank correlation functions $G_m(t)$. Their specific form can be obtained from analytical models (25,27,51) or from atomistic simulations (34,35). While in the former case explicit assumptions about the geometry of the molecular process are made, in the MD simulations the correlation function is directly calculated from the trajectory of the atomic coordinates of a particular molecular site.

In both approaches, the correlation function is given by the fluctuations of the EFG tensor about its mean value by

$$G_m(t) = \Big\langle [V_m^{(2)lab}(0) - \langle V_m^{(2)lab}\rangle]^* [V_m^{(2)lab}(t) - \langle V_m^{(2)lab}\rangle] \Big\rangle / (V_0^{(2)PAS})^2, \quad (4)$$

where the brackets indicate a time or ensemble average and $m = 0, \pm1, \pm2$. In Eq. 4, $V_m^{(2)}$ are the irreducible elements of the EFG tensor in the laboratory (lab) or principal axis system (PAS), respectively (13). The transformation from the laboratory system into the PAS is conveniently carried out using the Wigner rotation matrices $D^{(2)}_{m'm}(\Omega)$ tabulated elsewhere (13), which are functions of the three Euler angles $\Omega = (\alpha, \beta, \gamma)$. This leads to the result

$$G_m(t) = \sum_s \sum_{s'} V_s^{(2)PAS} V_{s'}^{(2)PAS} \Big\langle [D^{(2)}_{sm}(\Omega_{PL}; 0) - \langle D^{(2)}_{sm}(\Omega_{PL})\rangle]^* \times [D^{(2)}_{s'm}(\Omega_{PL}; t) - \langle D^{(2)}_{s'm}(\Omega_{PL})\rangle] \Big\rangle / (V_0^{(2)PAS})^2, \quad (5)$$

where the summation indices run from $-2,\ldots2$. The time-dependent matrix elements in this correlation function are functions of the Euler angles Ω_{PL} that describe transformation of the EFG tensor from the principal axis system (P) into the laboratory frame (L). This means that the motional model must contain the coordinate transformations, which has the advantage that each transformation may describe one specific molecular motion provided that these are sufficiently decoupled from one another.

Now to study the molecular dynamics of lipid chains in biological membranes, it is convenient to describe the transformation of the EFG tensor from the PAS into the laboratory system by the five transformations depicted in Fig. 1 (27,52). First, the diagonalized EFG tensor is transformed from its PAS into an internal system (I) using Euler angles Ω_{PI}. This transformation is sensitive to the *trans-gauche* isomerizations of the methylene groups. Second, a transformation to a molecular frame (M) is carried out that contains the motion of the hydrocarbon chain described by Euler angles Ω_{IM}. The third transformation converts the EFG tensor from the molecular frame into a system that is fixed to the time-dependent membrane normal $\mathbf{n}(t)$ (designated by N), allowing the inclusion of rotational and tilting motions affecting the entire lipid molecule through Euler angles Ω_{MN}. The fourth transformation leads into the system of the averaged membrane normal $\mathbf{n_0}$ (membrane director, D) and may thereby include collective motions described by Euler angles Ω_{ND}. Last, the fifth transformation describes the macroscopic orientation of the sample with respect to the external magnetic field aligned with the laboratory (L) system, which is time-independent as given by Euler angles Ω_{DL}. All these transformations can be calculated using the Wigner rotation matrices according to

$$D^{(2)}_{sm}(\Omega_{PL}, t) = \sum_r \sum_q \sum_p \sum_n D^{(2)}_{sr}(\Omega_{PI}, t) D^{(2)}_{rq}(\Omega_{IM}, t) \times D^{(2)}_{qp}(\Omega_{MN}, t) D^{(2)}_{pn}(\Omega_{ND}, t) D^{(2)}_{nm}(\Omega_{DL}). \quad (6)$$

Briefly, the Wigner rotation matrix elements constitute a group, and we can introduce their closure property to describe the resultant or overall transformation in terms of Euler angles Ω_{PL} using the rotation matrix elements for the various intermediate frame transformations (22), i.e., with Euler angles Ω_{PI}, Ω_{IM}, Ω_{MN}, Ω_{ND}, and Ω_{DL}.

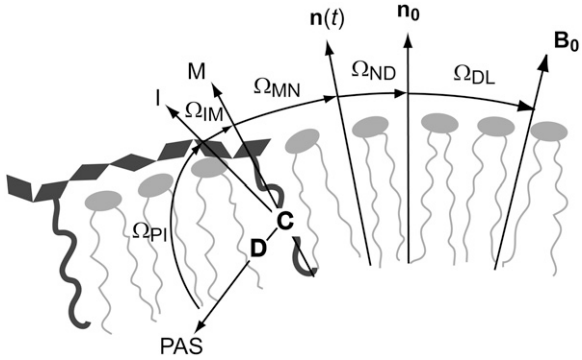

FIGURE 1 Schematic representation of transformations employed in generalized dynamics models for lipidated ras-d_{66} peptide in membranes. Each rotation is carried out by specific Euler angles that contain information about motional averaging on a specific timescale. For definitions of Euler angles and coordinate frames, see text.

Analytical models for dynamics of lipids and lipidated peptides

The theory presented so far allows for a simple separation of several dynamic processes associated with each coordinate transformation of the EFG tensor. In the following treatment, we shall describe the relaxation of ^{2}H spin states due to molecular and collective motions. To this end, a composite stochastic model describing order fluctuations due to molecular rotations together with slow collective bilayer deformations has been developed, and is briefly outlined here. For a more comprehensive description, we refer to the literature (24,25,27). In the model, the spectral density function is given by

$$J_m(\omega, \beta_{DL}) = J_m^{mol}(\omega, \beta_{DL}) + J_m^{coll}(\omega, \beta_{DL}) + J_m^{cross}(\omega, \beta_{DL}), \quad (7)$$

and includes terms for the molecular (*mol*) and the collective (*coll*) motions as well as a cross term (*cross*). The angle β_{DL} describes the orientation of the membranes with respect to the external magnetic field. The molecular-order fluctuations include the preaveraging of the coupling tensor due to faster segmental motions (transformations $P \rightarrow I \rightarrow M$), and involves the third subtransformation described above ($M \rightarrow N$).

Molecular motions

The expression for the spectral density is given by (22, 26,27,53)

$$J_m^{mol}(\omega,\beta_{DL}) = |\langle D_{00}^{(2)}(\Omega_{PI})\rangle|^2 \sum_q \sum_n \left| D_{0q}^{(2)}(\Omega_{IM}) - \frac{\eta_Q^{eff}}{\sqrt{6}}[D_{-2q}^{(2)}(\Omega_{IM}) + D_{2q}^{(2)}(\Omega_{IM})] \right|^2 \left[\langle |D_{qn}^{(2)}(\Omega_{MD})|^2 \rangle - |\langle D_{qn}^{(2)}(\Omega_{MD})\rangle|^2 \delta_{q0}\delta_{n0} \right] j_{qn}^{(2)}(\Omega_{MD};\omega) |D_{nm}^{(2)}(\Omega_{DL})|^2, \quad (8)$$

where $\delta_{m'm}$ is the Kronecker delta. The equation simplifies for C–^{2}H bonds for cases where the residual (effective) asymmetry parameter is $\eta_Q^{eff} \approx 0$. In Eq. 8, the molecular motions are described by the term $\left[\langle |D_{qn}^{(2)}(\Omega_{MD})|^2\rangle - |\langle D_{qn}^{(2)}(\Omega_{MD})\rangle|^2 \delta_{q0}\delta_{n0}\right] j_{qn}^{(2)}(\Omega_{MD};\omega)$, where the time-independent mean-squared amplitudes $\langle |D_{qn}^{(2)}(\Omega_{MD})|^2\rangle$ and the squared average $|\langle D_{00}^{(2)}(\Omega_{MD})\rangle|^2$ are separated from the time-dependent reduced spectral densities $j_{qn}^{(2)}(\Omega_{MD};\omega)$. Moreover, if one assumes an axially symmetric rotation of the molecule with a diffusion tensor having principal values of $D_\perp$ and $D_\parallel$, then the reduced spectral densities can be written as

$$j_{qn}^{(2)}(\Omega_{MD};\omega) = \frac{2\tau_{qn}^{(2)}}{1 + (m\omega\tau_{qn}^{(2)})^2}. \quad (9)$$

Here the correlation time is defined as

$$\frac{1}{\tau_{qn}} = \frac{\mu_{qn}}{\left\langle [d_{qn}^{(2)}(\beta_{MD})]^2 \right\rangle - \left\langle d_{qn}^{(2)}(\beta_{MD}) \right\rangle^2 \delta_{q0}\delta_{n0}} D_\perp + (D_\parallel - D_\perp) n^2, \quad (10)$$

where the symbols $d_{m'm}^{(2)}(\beta)$ are the reduced Wigner rotation matrix elements. The time-independent squared amplitudes of the motion can be calculated using a Clebsch-Gordon series as discussed by Trouard et al. (27):

$$|D_{m'm}^{(2)}(\Omega)|^2 = [d_{m'm}^{(2)}(\beta)]^2 = \sum_{j=0}^{4} c_{m'}^{(j)} c_m^{(j)} d_{00}^{(j)}(\beta). \quad (11)$$

The coefficients $c_m^{(j)}$ are defined as

$$c_m^{(j)} = (-1)^m \sqrt{2j+1} \begin{pmatrix} 2 & 2 & j \\ m & -m & 0 \end{pmatrix}, \quad (12)$$

with $\begin{pmatrix} j_1 & j_2 & j_3 \\ m_1 & m_2 & m_3 \end{pmatrix}$ being the Wigner 3-j symbol. The moments μ_{qn} are also calculated via a Clebsch-Gordon series,

$$\mu_{qn} = 6c_q^{(0)}c_n^{(0)}\langle d_{00}^{(0)}(\beta_{MD})\rangle + 5c_q^{(1)}c_n^{(1)}\langle d_{00}^{(1)}(\beta_{MD})\rangle + 3c_q^{(2)}c_n^{(2)}\langle d_{00}^{(2)}(\beta_{MD})\rangle - 4c_q^{(4)}c_n^{(4)}\langle d_{00}^{(4)}(\beta_{MD})\rangle, \quad (13)$$

where the term $\langle d_{00}^{(j)}(\beta_{MD})\rangle$ is generated via the Boltzmann distribution

$$\langle d_{00}^{(j)}(\beta_{MD})\rangle = \frac{\int_0^\pi d_{00}^{(j)}(\beta_{MD}) \exp[-U(\beta_{MD})/kT] \sin\beta_{MD} d\beta_{MD}}{\int_0^\pi \exp[-U(\beta_{MD})/kT] \sin\beta_{MD} d\beta_{MD}}. \quad (14)$$

A first-order potential of mean torque $U(\beta_{MD}) = -\lambda P_1(\cos\beta_{MD})$ is assumed, which represents the repulsive restoring force for a molecule that has been brought out of equilibrium, where $P_1(\cos\beta_{MD})$ is a Legendre polynomial of odd parity (27).

Finally, the term $|\langle D_{00}^{(2)}(\Omega_{PI})\rangle|^2$ is calculated from the experimentally determined order parameter S_{CD} via

$$S_{CD} = \left\langle D_{00}^{(2)}(\Omega_{PI}) \right\rangle D_{00}^{(2)}(\Omega_{IM}) \left\langle D_{00}^{(2)}(\Omega_{MD}) \right\rangle. \quad (15)$$

The fast order parameter $S_f^{mol} = \langle D_{00}^{(2)}(\Omega_{PI})\rangle$ is determined using Eq. 15, where $\langle D_{00}^{(2)}(\Omega_{MD})\rangle$ is the slow order parameter S_s^{mol}, which is determined from Eq. 14 and $\beta_{IM} = 90°$. The remaining term $|D_{nm}^{(2)}(\Omega_{DL})|^2$ in Eq. 8 describes the orientation of the membrane normal of the sample in the external magnetic field $\boldsymbol{B_0}$. Therefore, the fit parameters in the model for the molecular motions are $D_\perp$, $D_\parallel$, and λ, where the latter describes the strength of the repulsive restoring force in the potential of mean torque. As a modification of the original model (25), the strength of the potential of mean torque is adjusted to the chain position according to the order parameter. Expanding Eq. 30 of Petrache et al. (25) to linear order leads to the approximation $\lambda^{(i)} = \lambda_a S_{CD}^{(i)} + \lambda_b$, where λ_a and λ_b are adjustable parameters. In effect, we adopt an approach for the composite motion that contains elements of local motions with a position-dependent mean-torque potential.

Collective order fluctuations

In addition to the slow molecular fluctuations, collective motions may also contribute to the spectral density. The contribution due to relatively slow fluctuations of the local director with respect to the average director, i.e., the macroscopic bilayer normal, has been derived in the composite membrane deformation model (24,25,27). The spectral densities due to collective motions are represented by the terms (26)

$$J_m^{coll}(\omega,\beta_{DL}) = \frac{5}{2}|\langle D_{00}^{(2)}(\Omega_{PN})\rangle|^2 \frac{D_{coll}}{\sqrt{\omega}} \left[|D_{-1m}^{(2)}(\Omega_{DL})|^2 + |D_{1m}^{(2)}(\Omega_{DL})|^2 \right], \quad (16)$$

where the coordinate transformation $N \rightarrow D$ is expressed by $1/\sqrt{\omega}$. The only unknown in the model is the parameter D_{coll}, which describes the elasticity, viscosity, and temperature of the membrane. The terms $|D_{-1m}^{(2)}(\Omega_{DL})|^2$ and $|D_{1m}^{(2)}(\Omega_{DL})|^2$ represent the orientation of the sample in the membrane and are calculated from the angle between the average membrane normal and the external magnetic field. The term $|\langle D_{00}^{(2)}(\Omega_{PN})\rangle|^2$ is calculated from the experimental order parameter within the model for the collective motions:

$$S_{CD} = \left\langle D_{00}^{(2)}(\Omega_{PN}) \right\rangle \left\langle D_{00}^{(2)}(\Omega_{ND}) \right\rangle. \quad (17)$$

In this model, the term $\langle D_{00}^{(2)}(\Omega_{PN})\rangle \equiv S_f^{coll}$ represents the order parameter due to the fast internal motions plus the molecular motions. The factor $\langle D_{00}^{(2)}(\Omega_{ND})\rangle \equiv S_s^{coll}$ is the order parameter of the slow collective motions. To calculate $|\langle D_{00}^{(2)}(\Omega_{PN})\rangle|^2$ in Eq. 17, the value of the order parameter of the slow collective motions is required. Since the latter is not directly accessible, it is incorporated into the fitting parameter D_{coll}. The viscoelastic parameter D_{coll} is defined according to

$$D_{coll} = \frac{3}{5}\frac{kT}{\pi K^{3/2}(S_s^{coll})^2}\sqrt{\frac{\eta}{2}}, \quad (18)$$

where K is the elasticity constant and η is the viscosity of the membrane.

The cross term in the model is purely geometric and does not represent a correlation between molecular and collective motions. In the model, the cross term assumes the form

$$J_m^{cross}(\omega,\beta_{DL}) = \frac{S_{CD}^2}{S_s^2}\left\{J_{01}^{cross}(\omega) + \frac{3}{2}\left[J_{-21}^{cross}(\omega) + J_{21}^{cross}(\omega)\right]\right\}\left[3d_{0m}^{(2)}(\beta_{DL})^2 + d_{-2m}^{(2)}(\beta_{DL})^2 + d_{2m}^{(2)}(\beta_{DL})^2\right]$$
$$+ \left\{J_{02}^{cross}(\omega) + \frac{3}{2}\left[J_{-22}^{cross}(\omega) + J_{22}^{cross}(\omega)\right] + \frac{3}{2}\left[J_{00}^{cross}(\omega) + 3J_{20}^{cross}(\omega)\right]\right\}\left[d_{-1m}^{(2)}(\beta_{DL})^2 + d_{1m}^{(2)}(\beta_{DL})^2\right], \quad (19)$$

where $J_{qn}^{cross}(\omega)$ is defined by

$$J_{qn}^{cross}(\omega) = \left[\left\langle |D_{qn}^{(2)}(\Omega_{MN})|^2 \right\rangle - |\langle D_{qn}^{(2)}(\Omega_{MN})\rangle|^2\delta_{q0}\delta_{n0}\right] \times \frac{5}{3}D_{coll}\sqrt{\frac{\tau_{qn}\left[1+\sqrt{1+(\omega\tau_{qn})^2}\right]}{1+(\omega\tau_{qn})^2}}. \quad (20)$$

All necessary terms can be determined as described above.

Finally, we note that both the molecular and the collective contributions of the analytical model do not contain the fast internal motions of the molecule due to *trans-gauche* isomerization. These motions are assumed to be extremely fast and approximately independent of the sample orientation. Therefore, an additional fitting parameter R_{int} is introduced that is added to the total relaxation rate.

Calculation of angular-dependent ^{2}H relaxation rates from molecular dynamics simulations

Equation 4 provides a general definition for the correlation function of motion of an irreducible EFG tensor component. The static EFG tensor for C–^{2}H bonds is axially symmetric to a good approximation ($\eta_Q \approx 0$); therefore, the $V_{\pm2}^{(2)PAS}$ elements of the EFG tensor vanish and the correlation functions are given as

$$G_m(n\Delta t) = \langle D_{0m}^{(2)}[\Omega, n\Delta t] D_{0m}^{(2)*}[\Omega, 0]\rangle - |\langle D_{0m}^{(2)}(\Omega)\rangle|^2, \quad (21)$$

where n is the number of time steps Δt in the simulation that are considered. The angular brackets $\langle \ldots \rangle$ indicate a time or ensemble average assuming stationary random functions. As described above, the EFG components within the laboratory frame are modulated by a hierarchy of motions, including local isomerization of the acyl groups, molecular motions, and collective motions due to quasielastic properties of the bilayer. In contrast to the simplified analytical model described above, all-atom MD simulations do not require additional mathematical simplification. Analysis of the MD simulation typically yields the spherical harmonics that describe the time-dependent orientation of the C-^{2}H bond vector in the laboratory system in terms of the Euler angles $\Omega(t) = (\alpha, \beta, \gamma)$. These can be converted to the Wigner rotation matrices for $m' = 0$ using

$$D_{0m}^{(2)}(\alpha,\beta,0) = \sqrt{\frac{4\pi}{5}}Y_m^{(2)}(\beta,\alpha). \quad (22)$$

The spectral density function is then obtained from the correlation function using a discrete Fourier transform

$$J_m(\omega_n,\beta_{DL}) = 2\sum_{n=0}^{l-1} G_m(n\Delta t,\beta_{DL})\cos(\omega_n n\Delta t)\Delta t, \quad (23)$$

where l is the number of time intervals of the correlation function and Δt is the time increment. The results presented here had $l = 100\,000$ and $\Delta t = 1$ ps. The discrete frequencies are calculated according to

$$\omega_n = 2\pi\frac{n}{l\Delta t}. \quad (24)$$

To save computational time, only the director frame ($\beta_{DL} = 0$) spherical harmonics were calculated from the MD simulation. Using the transformation properties of spherical harmonics under rotations, all spectral densities at any given angle were calculated by (25)

$$J_m(\omega_n,\beta_{DL}) = d_{0m}^{(2)}(\beta_{DL})^2 J_0(\omega,0°) + [d_{-1m}^{(2)}(\beta_{DL})^2 + d_{1m}^{(2)}(\beta_{DL})^2]J_1(\omega,0°) + [d_{-2m}^{(2)}(\beta_{DL})^2 + d_{2m}^{(2)}(\beta_{DL})^2]J_2(\omega,0°). \quad (25)$$

Equation 25 is only valid for axially symmetric molecules and an axially symmetric distribution about the director axis (25).

RESULTS

Order parameters of ras chain modifications in membrane environment

Measurement of the angular dependence of solid-state ^{2}H NMR spectra and corresponding ^{2}H relaxation rates was carried out on macroscopically oriented membranes containing ras peptides at a 1:15 peptide/lipid molar ratio. A typical set of ^{2}H NMR spectra recorded at 40°C as a function of the tilt angle between the membrane normal and the external magnetic field $\boldsymbol{B_0}$ is shown in Fig. 2. At 0° tilt angle, i.e., with the membrane normal aligned parallel to the external field, the largest dispersion of residual quadrupolar couplings is observed. Upon rotation of the oriented sample relative to the magnetic field, the quadrupolar splittings

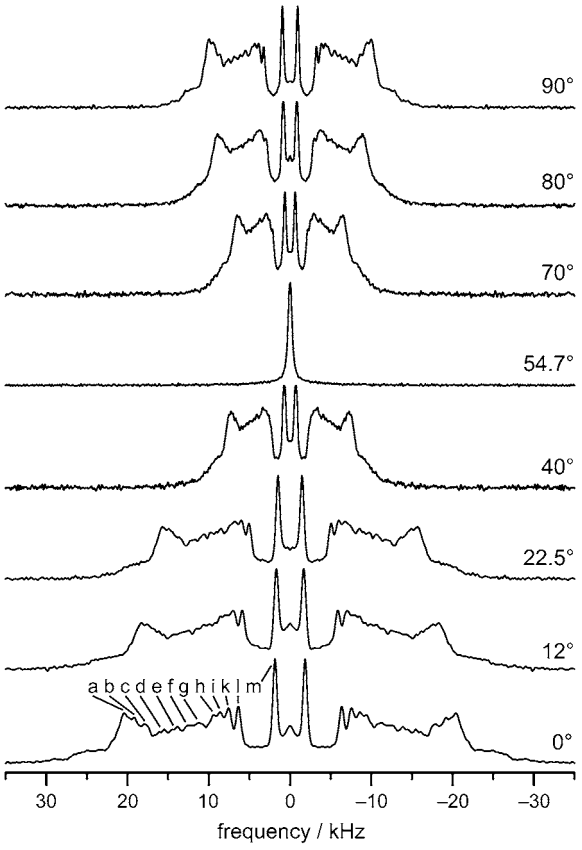

FIGURE 2 Experimental 115.1 MHz solid-state ^{2}H NMR spectra of ras-d_{66} peptide in DMPC bilayers (1:15) at 40°C as a function of orientation of membrane normal to external magnetic field. The largest dispersion of quadrupolar splittings is obtained at 0° tilt angle with all Pake doublets converging to a single peak at the magic angle (54.74°). Thereafter, the quadrupolar splittings increase in absolute magnitude and are scaled by −1/2 of the 0° value at 90°. Letters refer to quadrupolar splittings assigned to the carbon atoms in the chain. Residual quadrupolar couplings of the acyl-chain carbons are indicated by letters.

systematically decrease and collapse into a single isotropic peak at the magic angle (54.74°). The splittings then change sign, and at the 90° value, i.e., with the membrane-normal perpendicular to the external field, they are scaled by −1/2 of the 0° value. This scaling property of the quadrupolar couplings is well described by the second Legendre polynomial. The fact that a very narrow line is obtained for the 54.74° orientation of the membranes confirms that the alignment of the sample was very good.

From the angular-dependent ^{2}H NMR spectra, the individual quadrupolar splittings for the methylene groups in the peptide lipid chain can be obtained. However, due to the limited resolution of the ^{2}H NMR spectra, especially at tilt angles $>\sim25°$, a lineshape simulation was carried out to obtain the individual splittings. In these simulations, a superposition of 12 Lorentzian doublets was used to fit the experimental spectra. From the quadrupolar couplings the order parameters of each of the methylene groups were calculated using Eq. 1. For validation of the fitting procedure, the order parameters were compared to those obtained from the de-Paked powder spectra analyzed previously (17). A plot of the order parameters for each ras peptide chain segment is shown in Fig. 3 *a* (*squares*). Numerical values are given in Table 1. It is interesting to note that the order profile is somewhat flatter compared to those of saturated phospholipid chains (54). However, similar order profiles have also been obtained for the *sn*-1 chain of polyunsaturated phospholipid membranes (55,56). Such polyunsaturated membranes are well known to be very flexible and highly dynamic (32,55,57–59). Thus, the order profile obtained for the lipid modification on the ras peptide provides a first hint that these lipid chains are also flexible and highly dynamic. This is consistent with ideal mixing of the ras peptide with the host DMPC bilayer matrix, with no phase separation into raftlike domains.

The peptide chain order parameters obtained from the MD simulation, are also shown in Fig. 3 *a* for the Cys-181 chain (+) and for the Cys-186 chain (×). The general shape of the calculated order parameter profiles differs from the experimental result. Another very striking feature of the simulated profile is that the two hexadecyl chains have very different order parameters in the upper half of the chains. While a rather linear increase in the experimentally obtained order parameters is obtained for the chain methylenes until the plateau peak is reached, the order parameters from the MD simulation follow a more curved profile. In addition, the calculated order parameters are somewhat higher for the bottom part of the chain and significantly lower for the C1 segment at the top of the acyl chain. Analysis of the C-^{2}H orientational fluctuations in the simulation show that the low-order parameter at C1 arises not from greater disorder versus its neighbors, but rather from a geometrical effect, i.e., the C-^{2}H bond vector distribution is not peaked in the plane of the membrane. This could arise from a conformational preference of the cysteine side chain; however, it could also

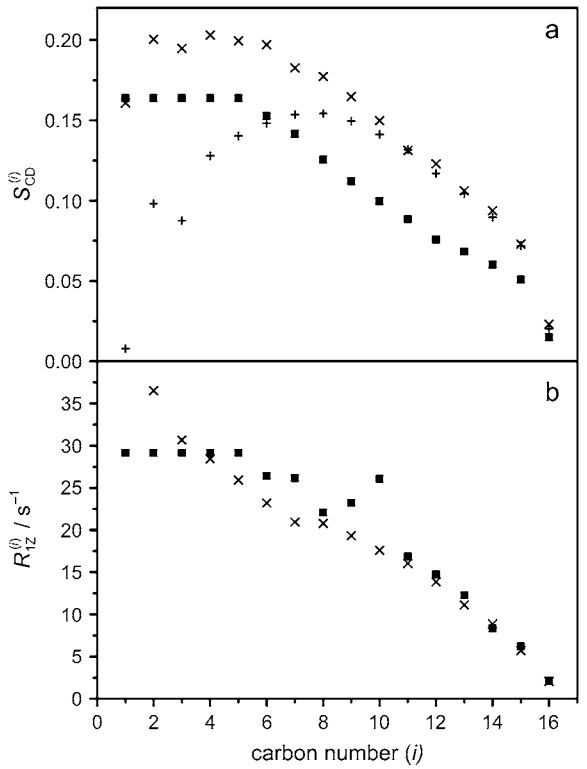

FIGURE 3 Comparison of order parameters and spin-lattice relaxation rates for hexadecyl chains of ras-d_{66} peptide/DMPC (1:15) bilayers obtained from solid-state ^{2}H NMR measurements and molecular dynamics simulations. (*a*) Order parameters $S_{CD}^{(i)}$ and (*b*) relaxation rates $R_{1Z}^{(i)}$ for ras-d_{66} peptide at 40°C plotted as a function of the chain methylene segment (*i*). Solid symbols represent experimentally determined values whereas crosses show the same quantities calculated from MD simulations (+ for lipid modification at Cys-181, × for lipid modification at Cys-186). The relaxation rate for C1 from the simulation is 55.97 s^{-1} and is omitted for clarity. A plateau is found in the experimental data because spectral resolution is lacking for the upper chain segments. Order parameters and relaxation rates were obtained for oriented membrane stacks with the bilayer normal (director) parallel to the external magnetic field.

indicate inadequate sampling of the peptide backbone. The lack of convergence of the order parameter at this position is further suggested by the large statistical error in its calculation (≈40% of the mean at C1, by far the largest of any segment). It also should be recalled that the experimental order parameters were not assigned to the respective carbon in the chain, but rather plotted according to increasing quadrupolar splitting. In contrast, the MD simulation provides the true order parameter profile with the correctly assigned value for each carbon atom.

Spin-lattice relaxation rates of ras chains in membrane bilayers

To obtain further insights into the dynamics of the lipid modifications of the ras-d_{66} peptide, spin-lattice relaxation rate measurements were carried out. Profiles of R_{1Z} against the chain segment index are presented in Fig. 3 *b* and Table 1

TABLE 1 Summary of the order parameters and corresponding R_{1Z} relaxation rates at 0° orientation for membrane associated ras-d_{66} peptides in DMPC membranes at 40°C

Peak*	$\lvert S_{CD}\rvert$	R_{1Z} /s^{-1}
a	0.1638	29.15 ± 0.97
b	0.1527	26.41 ± 0.54
c	0.1415	26.15 ± 0.95
d	0.1255	22.06 ± 0.59
e	0.1121	23.22 ± 0.87
f	0.0997	26.08 ± 0.74
g	0.0885	16.89 ± 0.27
h	0.0758	14.74 ± 0.32
i	0.0684	1.27 ± 0.30
k	0.0602	8.34 ± 0.12
l	0.0508	6.21 ± 0.14
m	0.0149	2.13 ± 0.04

*The letter designations of the peak assignments correspond with those in Fig. 2.

for the parallel orientation of the membrane normal $\mathbf{n_0}$ to the external magnetic field $\boldsymbol{B_0}$. For comparison, site-specific R_{1Z} relaxation rates from the MD simulation are provided in Fig. 3 *b*. It can be seen that much better agreement between simulation and experiment is obtained for the relaxation rates as opposed to the order parameters (S_{CD}). Importantly, the correspondence of the theoretical MD simulation results with the experimental R_{1Z} rates suggests that all stochastic motions and conformational changes that contribute to the spin-lattice relaxation are well sampled in the MD simulations within 100 ns. The exception is at the top of the acyl chain, where the simulated rates are much higher for the C1 and C2 methylenes. This could indicate a shortcoming in the force field that does not allow sufficiently rapid conformational transitions in the cysteine group or cysteine-hexadecyl linkage. Alternatively, there could be a significant contribution from motions not present in the simulation system, e.g., director fluctuations suppressed by the small dimension of the simulation cell. Moreover, an outlier data point is observed in the experimental rates for carbon 10. We emphasize that the experimental relaxation rates are model free and are merely plotted according to their decreasing quadrupolar splitting. By contrast, the rates obtained from the MD simulations are correctly assigned, which may explain the outlier in the experimental data, because it may correspond to a carbon of the upper chain.

A second interesting aspect is that while the order parameters of the two ras lipid chains differ appreciably, their simulated relaxation rates are rather similar. This is further demonstrated in Fig. 4, where the correlation functions of the Cβ methylene group of the side chains of Cys-181 and Cys-186 are plotted. From the simulated order parameters, it is obvious that the orientations of the two cysteines appear to be nonidentical on the MD timescale. For these two cysteine residues, order parameters of −0.126 and −0.00688 are determined from the simulation. On the other hand, the similarity of the correlation functions shows that relaxation is

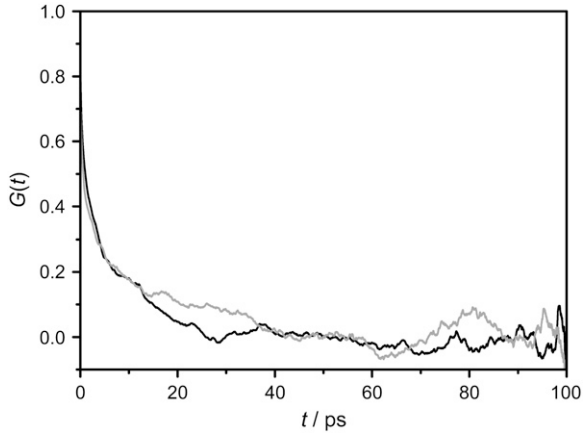

FIGURE 4 Correlation functions for Cys-181 (*black*) and Cys-186 (*gray*) Cβ carbons of the amino-acid side chains for ras peptide in DMPC bilayer at a 1:15 molar ratio determined from the molecular dynamics simulation. The MD simulation corresponds to a temperature of 40°C.

largely governed by the motions independent of the order parameter (plateau of the correlation function). Due to geometrical effects the mean-squared values differ significantly. Yet upon subtraction, the rates and motional amplitudes relative to the mean values are seen in fact to be rather similar.

Previous analyses of pure phospholipid membranes have found that the relaxation rate often exhibits a linear dependence on the square of the order parameter (27). While the physical reason for this interesting behavior is still under discussion, it has been shown to be a common feature for disaturated phospholipids. The experimental square-law plots for the ras alkyl chains in a DMPC-matrix is shown in Fig. 5 *a* as a double logarithmic graph. Clearly, the experimental data do not show the square-law behavior over the full chain length, while the simulated data points look more linear. The $R_{1Z}^{(i)}$ versus $|S_{CD}^{(i)}|^2$ plot is given in Fig. 5 *b*. As already seen for powder-type samples, the $R_{1Z}^{(i)}$ versus $|S_{CD}^{(i)}|^2$ plot for the ras-d_{66} hydrocarbon chains departs from the linear dependence and shows a bent shape with a steeper slope. Previous investigations of phospholipids have shown that the slope of the square-law plots is correlated with the elastic properties of the membranes (25,27). Since the macroscopic elastic properties of membranes are a consequence of the molecular dynamics and packing, combined measurements of relaxation times and order parameters are well suited to relate atomic-level properties to the macroscopic behavior of biological materials.

In fact, a bent shape of the square-law plots, together with a steeper slope, is the typical signature of soft and elastic membranes made from highly mobile and flexible chains. These membranes typically consist of polyunsaturated phospholipids (59) or phospholipids in the presence of a detergent (17,60). This behavior of the ras lipid modifications was first observed in multilamellar vesicle preparations, and is exactly reproduced in oriented membranes (17,19). Interestingly, the square-law plots of the surrounding lipid matrix were only marginally influenced (17,19). Therefore, it was previously

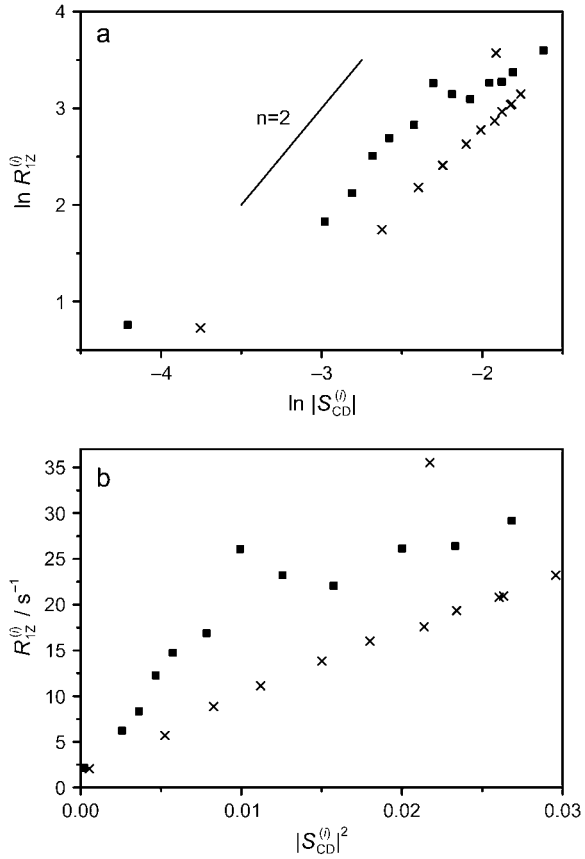

FIGURE 5 Square-law functional dependence of ^{2}H NMR spin-lattice relaxation rates $R_{1Z}^{(i)}$ on corresponding squared order parameters $|S_{CD}^{(i)}|^2$ measured for hexadecyl chains of ras-d_{66} peptide at 40°C at a magnetic field of 17.6 *T*. Experimental data (■) and values obtained from molecular dynamics simulations (×) are shown. Data are shown for bilayers on planar supports with the normal (director) aligned parallel to the external magnetic field. The outlier data point in the simulated curve represents the average of carbons C1–C5 corresponding to the plateau peak of the experimental data.

concluded that the specific slope of the square-law plot of the ras lipid modifications is a consequence of the insertion of the ras backbone into the lipid water interface of the membrane. This provides free volume underneath, which is occupied by larger amplitude motions of the ras chains (15–17,19). In our previous analysis, we also emphasized the matching of the ras chains with those from the surrounding lipid matrix, which is observed for DMPC (16,17). The square-law plot from the MD simulation shows a less pronounced curvature, which is caused by the different order parameters calculated in the MD simulation of the ras chains (see Fig. 3).

Orientation-dependent relaxation of ras chains in membrane bilayers

A wealth of information about the dynamics of the lipid acyl chains is contained in the orientation dependence of the spin-lattice relaxation rates (25,27,61,62). In the solid state, the

relaxation of the excited spin states is a quantity that depends on the orientation of a molecular site with respect to the external magnetic field. Provided that appropriate models are employed, detailed information about the molecular motions can be deduced from such data. For a qualitative evaluation of the relaxation rates as a function of orientation, it is useful to know that with increasing amplitude of motions the angular dependence of the relaxation rates is less pronounced.

We measured the spin-lattice relaxation of ras-d_{66} heptapeptides in a DMPC host membrane at a relatively high 17.6 T magnetic field. To this end, the membranes containing ras peptides were stacked between glass plates and rotated to the desired angle between the membrane normal and external magnetic field using the goniometer NMR probe. Experimental spin-lattice relaxation rates are given in Fig. 6 for various chain positions as data points. At first glance, rather little angular dependence of these rates is observed in agreement with highly flexible and mobile lipid modifications of ras. Even for the upper-chain segments corresponding to the unresolved plateau peak, only a very weak angular dependence of R_{1Z} is measured.

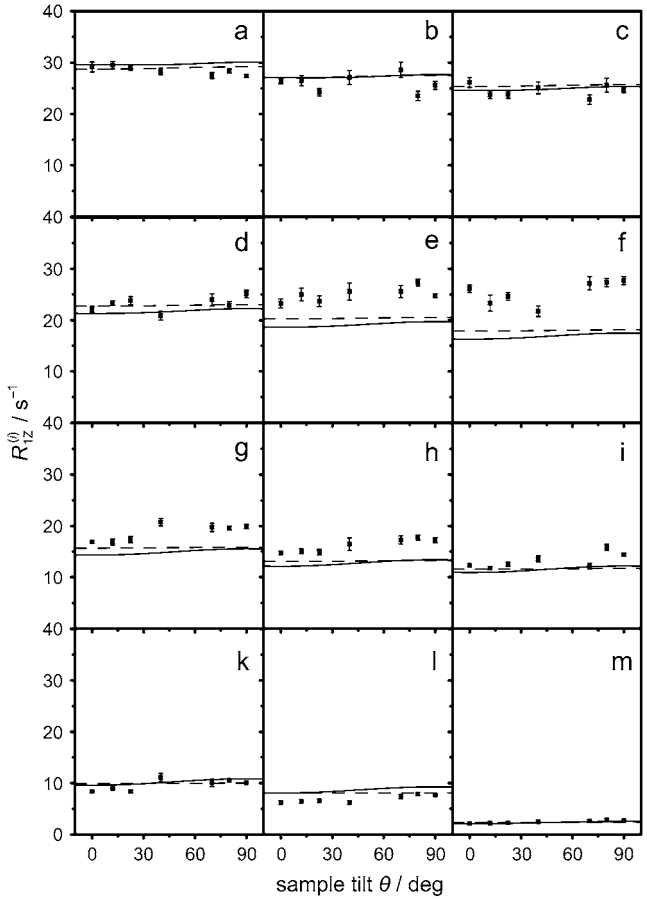

FIGURE 6 Simultaneous fit of analytical models for experimental ^{2}H NMR spin-lattice relaxation rates $R_{1Z}^{(i)}$ determined for ras-d_{66} chains in oriented DMPC bilayers as a function of angle between the lamellar normal and external magnetic field of 17.6 T. Experimental relaxation rates at 40°C are given as data points, and best fits to the molecular and composite membrane deformation models correspond to red and black lines, respectively. Panels refer to the residual quadrupolar couplings, i.e., representing different carbon positions, of the ras-d_{66} chains (compare to Fig. 3).

For a quantitative evaluation of the data obtained at a single frequency of 115.1 MHz, we followed two complementary strategies. First, the analytical model derived in Theory (see above) was applied. Either the relaxation rates were explained solely by use of the molecular model (Eq. 8), or the molecular model in combination with the composite membrane deformation terms was used (Eqs. 8, 16, and 19). We recall that the R_{1Z} relaxation rates of membrane lipid chains are frequency-dependent (26), so that this approach must be regarded as a first approximation. Using these closed-form analytical models, a simultaneous fit of the angular dependence of the relaxation of the ras-d_{66} peptide chains for all resolved peaks was carried out. As outlined in Theory (see above), the molecular model contains five independent parameters, whereas the full composite model has six parameters. These were determined by simultaneously fitting the relaxation rates measured for the 12 individual chain methylene and methyl signals from the ras lipid modifications. The results of both models are shown in Fig. 6, with a summary of the fitting parameters given in Table 2. No real differences in the quality of the fits are observed for the two models as indicated by rather close RMSD values. The fit is particularly good for the lower (C11–C16) and the upper (plateau through C8) chain segments. In the middle of the ras chains, the agreement between experimental data and the analytical model is relatively poor. This is exactly the region where the angular dependence of the relaxation rates changes its slope from monotonically decreasing for the upper chain to monotonically increasing for the lower part of the ras chains.

The orientation dependence of the ras-d_{66} chain relaxation rates can also be obtained from the MD simulations. From the trajectory of each atom in the simulation, the correlation function of motion of the C–^{2}H bond vectors in the hexadecyl chains of the ras-d_{66} peptide was calculated using Eq. 21. Representative correlation functions for the C4, C8, C12, and C16 carbons in the hexadecyl chain for all projection indices

TABLE 2 Fitting parameters for the molecular and composite membrane deformation models applied to ^{2}H NMR R_{1Z} relaxation rates of hexadecyl chain modifications of membrane associated ras-d_{66} peptides

Parameter	Molecular model	Composite membrane deformation model
$D_{\|\|}/10^9$ s^{-1}	83,500*	2.09
$D_{\perp}/10^5$ s^{-1}	2.24	4.53
λ_a/k_BT	1.99	31.61
λ_b/k_BT	0.71	1.71
$D/10^{-6}$ s$^{1/2}$	—	9.26
R_{int}/s^{-1}	1.57	0.33
RMSD	2.348	2.752

*In the molecular model, $D_{\|\|}$ cannot be determined with high precision from the fit.

$m = 0$, 1, and 2 are provided in the Supplementary Material. Since the MD simulation reproduces the experimental relaxation in the director frame relatively well, the angular dependence of the relaxation rates should also come out rather exact. The comparison of experimental and simulated data is shown in Fig. 7. It should be emphasized that the absolute magnitudes of the simulated relaxation rates were not corrected by an arbitrary scaling factor, but represent the true calculated relaxation rates from the MD simulation. Very similar to the analytical model, the MD simulation describes the orientational dependence of the spin-lattice relaxation for the lower part of the ras chain (segments C11–C16) very well. This was already seen in the plot of the relaxation rates as a function of the chain segment shown in Fig. 3 *b*. For the upper-chain segments, the agreement between experiment and simulation is not quite as good. However, the change in slope approximately at the C8 methylene segment of the chain is also reproduced.

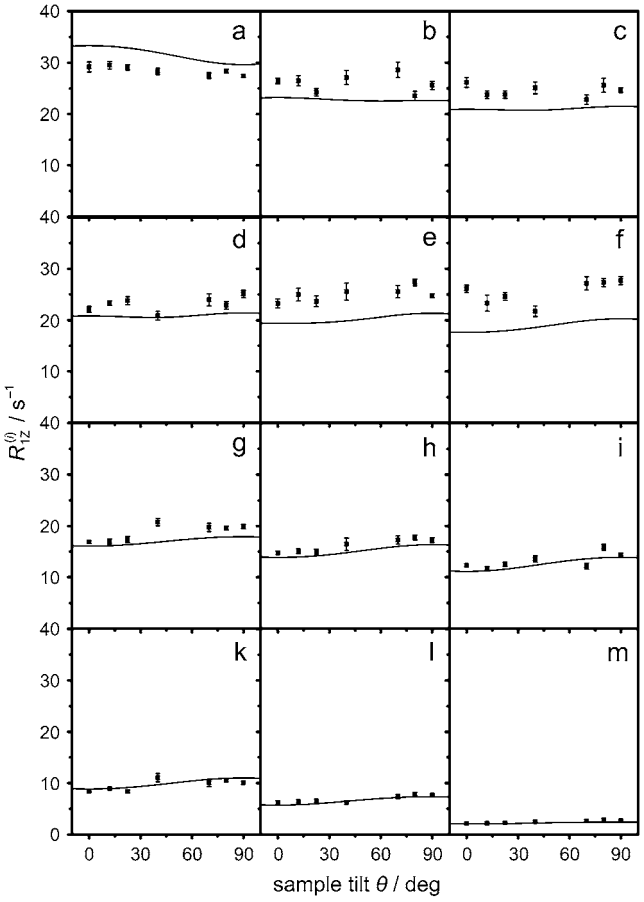

FIGURE 7 Angular dependence of ^{2}H NMR spin-lattice $R_{1Z}^{(i)}$ relaxation rates for ras-d_{66} chains in DMPC bilayer obtained from molecular dynamics simulations. Relaxation rates were simulated for an external magnetic field of 17.6 *T*, and are plotted as a function of angle between the membrane normal (director) and the external magnetic field. Experimental spin-lattice relaxation rates at 40°C are designated by data points. Panels represent the residual quadrupolar couplings due to the methylene groups of the ras-d_{66} chains.

DISCUSSION

Deuterium NMR spectroscopy and molecular dynamics simulations have both contributed a large body of data to characterizing the molecular structure and dynamics of biological samples, including in particular lipid membranes with bound peptides or associated proteins (13,23,63–69). Sample deuteration of lipids or peptides is directly accomplished by chemical synthesis, and one-dimensional solid-state ^{2}H NMR spectra are relatively straightforward to acquire. The experimental quantities obtained from these measurements, such as motionally averaged (residual) quadrupolar couplings and relaxation rates, are sensitive to the orientation and dynamics of the EFG tensor aligned along the C-^{2}H bond. Both structural and dynamical information are acquired at the atom-specific level for disordered liquid-crystalline membranes. For simulating such experimental ^{2}H NMR data, in general two approaches are possible: either one can adopt an approximate model that can be solved exactly (22), or one can consider a more exact all-atom force field that requires an approximate numerical solution (23). Both approaches are valuable, as the former renders the motions in an heuristic fashion that is easily understood, whereas the MD simulations embody a more accurate description of the interactions giving rise to the complex dynamical behavior. Both approaches place the molecular behavior firmly within the context of existing knowledge of interatomic and intermolecular forces. To the extent that the results converge, our confidence in the interpretation of experimental data is increased. In particular, MD simulations have advanced significantly in recent years (29). Currently atomistic simulations of >100 ns are routine and a number of experimental quantities are precisely reproduced (70–73) Here, we have used both strategies to elucidate the structure and dynamics of the chain modifications of a membrane-associated ras heptapeptide from the C-terminus of the human oncogenic N-ras protein.

Order parameters and dynamical nanostructure of ras peptide chains

Experimentally, the dynamic ras structure was investigated by analyzing ^{2}H NMR order parameters of the deuterated ras peptide chains. The order parameter profiles of saturated phospholipid chains are rather well understood, whereas less information is available regarding the interpretation of the order parameters of lipidated proteins. We have pointed out earlier that the order parameters of the ras lipid chains are significantly smaller than those of the DMPC host matrix (16,17). In addition, the ras chain order parameters plotted versus methylene position in the chain exhibit a somewhat unusual shape, which is reminiscent of the *sn*-1 chain of *sn*-2 polyunsaturated phospholipid membranes (55,56,74). Generally speaking, the lipid chain order parameters depend on the lateral pressure profile as determined by the balance of

attractive and repulsive forces in the bilayer membrane. The insertion of the ras peptide into the lipid membrane clearly disturbs this balance. This results in a modified order profile of the ras chains that is characteristic for highly mobile and disordered chains. It is known from ^{1}H magic-angle spinning NOESY studies that the backbone of ras is localized to the lipid water interface of the membrane, while the hydrophobic side groups and lipid chains are inserted into the membrane interior (15,16). This creates free volume in the membrane underneath the peptide backbone that accommodates the large amplitude motions of the amino-acid side chains and lipid chains of ras. Interestingly, the order parameters of the host membrane lipids are only very marginally perturbed, suggesting that most of the volume must be occupied by the ras chains (17). This is indicated by the relatively low order parameters of the peptide chains.

First we note that the order parameter plot for the ras chains obtained from the MD simulation shows some significant alterations compared to the experimental data. Several reasons for this discrepancy can be identified. The analysis of the ^{2}H NMR spectra rests on the assumption that order parameters gradually increase from the end of the chains to the top. This appears to be a reasonable assumption for phospholipids in planar membranes, but might be different for the peptide chains. In particular, geometric constraints on the upper methylene segments may render the order parameters small, which then do not report on the motional amplitude, but rather the scaling of the quadrupolar splitting by the fixed geometry. Second, the sampling of conformations in the MD simulation is somewhat limited, since trajectories for only four peptide molecules are available. Thus, the full conformational space of the ras chains may not have been sampled within the 100 ns of simulation. Despite the apparent discrepancy between simulated and experimental data, however, the average order parameters of the chains are very similar for the simulated and experimental values. This may suggest that the assumption of a gradual order increase from the bottom to the top of the chain may be an oversimplification. Third, the amplitudes of the CH_2 motions of the ras chains reflected in the experimental order parameter may also be influenced by collective motions of larger membrane patches, which are not contained in the simulation of 32 DMPC molecules in each leaflet. Such motions would possibly also be too slow to be sampled in the MD simulation. However, slow collective motions can produce amplitudes of up to 30°, which significantly decreases the experimental order parameters. The fact that such slow motions could actually play a role in the system is further supported by the comparison of the experimental and simulated relaxation rates. While these motions are per se not included in the MD simulations, they also do not play a significant role for the relaxation rates at a relatively high Larmor frequency of 115.1 MHz. Consequently, relatively good agreement between simulated and experimental relaxation rates is observed (Fig. 3 *b*). Additionally, Fig. 4 shows explicitly that the correlation function plateau values, which are related to the order parameter, can be different while the overall correlation functions, especially those regions that determine the relaxation rate, are quite similar.

Structural dynamics of ras chain modifications—continuum picture

In the other experimental part of this study, we extracted complementary detailed information about the ras chain dynamics from spin-lattice relaxation rates. These rates were analyzed by means of molecular and composite membrane deformation models, as well as MD simulations. The composite membrane deformation model has been successfully applied to phospholipid chains, and has provided comprehensive information about the details of the molecular dynamics (24–27). Although not substantiated here in detail, the model should also be applicable to lipidated membrane-associated peptides. In principle, the same five coordinate transformations that convert the EFG tensor from its principal axis system (PAS) into the laboratory frame apply for the peptide (Fig. 1). Compared to phospholipid molecules, the ras peptide has an approximately twofold larger molar mass, in addition to the completely different chemical structure of the lipidated molecule. This should lead to significant variations for the parameters in the composite membrane deformation model compared to phospholipids. Yet the applicability should not be compromised, since the general structure of the host membrane is only marginally affected by ras insertion (17). Compared to previous analyses, a small modification of the model was introduced to account for the highly curved and steep square-law plot observed for the ras chains, in contrast to the nearly linear dependence observed for pure phospholipid chains. The parameter λ that describes the potential of mean torque was adjusted to increase with the order parameter in a linear fashion; thus, each chain methylene segment experiences a different repulsing restoring potential. With this minor modification, reasonable fits of the angular dependence of the spin-lattice relaxation rate could be obtained using either a molecular or a composite membrane deformation model.

At a high magnetic field of 17.6 T, the contribution from somewhat slower motions of the ^{2}H spin-lattice relaxation rates is diminished (34,75). An estimation of the spectral density at 17.6 T reveals that motions with correlation times of 100 ns only contribute a few percent to the spectral density. This suggests that relaxation parameters may be described on the basis of slow order fluctuations due mainly to molecular motions, without explicitly considering collective motions. We have applied two models that either include or neglect these somewhat slower dynamical modes. While the quality of the fitting procedure is rather similar for both models, the model that considers molecular motions only produces somewhat higher values for $D_{\|}$ and $D_{\perp}$ while the other parameters are comparable (Table 2).

For the analytical model, the interesting parameters are the principal components of the anisotropic diffusion tensor $D_{\parallel}$ and $D_{\perp}$. For the ras-d_{66} peptide in the DMPC bilayer at a temperature of 40°C, the composite model yields $D_{\parallel} = 2.1 \times 10^9\ s^{-1}$ and $D_{\perp} = 4.5 \times 10^5\ s^{-1}$. These parameters should be compared with what is known about the dynamics of membrane-associated peptides. Unfortunately, little data are available on the dynamics of integral or peripheral membrane peptides (76). Many studies on those peptides focus on structural aspects and are therefore carried out at low temperature to freeze out molecular motions. Perhaps the most structural and dynamical details are available for gramicidin D (65), for which a membrane structure with atomic resolution exists (77). ^{2}H NMR relaxation has been used to study the anisotropic molecular dynamics of gramicidin in membranes (28). For the membrane-inserted gramicidin helix $D_{\parallel} = 0.15 \times 10^9\ s^{-1}$ and $D_{\perp} = 1.7 \times 10^5\ s^{-1}$, which can be compared with the data for the ras peptide determined here. A faster axially symmetric rotation is observed for the hydrocarbon chains of the membrane-associated ras, which also has a smaller molar mass (≈1.3 kDa vs. ≈1.8 kDa). In comparing these data, one also needs to consider that the molecular motions of gramicidin were determined from the deuterated amides in the peptide backbone. By contrast, for the ras peptide the lipid chain modifications report the molecular mobility and may include additional contributions from internal motions of the molecule.

Moreover, we can compare our parameters for the ras peptide with those determined for the acyl chains in phospholipid membranes (25). For pure DMPC membranes at a temperature of 40°C, the composite model yields $D_{\parallel} = 4.5 \times 10^9\ s^{-1}$ and $D_{\perp} = 73 \times 10^5\ s^{-1}$. The molecular dynamics of the membrane-bound ras peptide are roughly comparable to that of the membrane lipids. However, the off-axial rotational diffusion constant $D_{\perp}$ for the ras-d_{66} chains is only ~6% of that for the pure DMPC, indicating that it may be strongly tethered to the aqueous interface. In fact, this might be expected, since the chains are bound to the comparatively large heptapeptide, which is nearly twice the mass of DMPC. On the other hand, the axial diffusion constant $D_{\parallel}$ is ~50% of the value for DMPC, which may be consistent with a slightly slower motion of the ras-d_{66} molecule. In general the axial diffusion constant is not well determined from the fits, and this result may require some caution. Lastly, for the viscoelastic D_{coll} parameter of the collective motions, a value of $6.81 \times 10^{-6}\ s^{1/2}$ has been reported for DMPC, which is slightly less than for ras. As D_{coll} describes the elasticity, viscosity, and temperature of the membrane, the observed changes can be attributed to a slight increase in these parameters in the vicinity of the ras peptide, or to a different order parameter S_s^{coll} as described by Eq. 18.

To provide an additional benchmark, the dynamical behavior of the ras chains can be contrasted with phospholipids in bilayers containing cholesterol. In the case of DMPC/cholesterol (1:1) bilayers, values of $D_{\parallel} = 5.4 \times 10^9\ s^{-1}$ and $D_{\perp} = 4.0 \times 10^5\ s^{-1}$ have been obtained for the phospholipid component (24). By contrast, the rotational dynamics of the rigid cholesterol molecule in the liquid-ordered state are appreciably slower. Rotational diffusion coefficients of $D_{\parallel} = 0.42 \times 10^9\ s^{-1}$ and $D_{\perp} = 0.83 \times 10^5\ s^{-1}$ have been obtained for cholesterol in DPPC bilayers at 30°C in the short correlation time regime (78). The difference between the rotational dynamics of the DMPC chains and cholesterol can be simply explained in terms of internal motions in the former case (79). For the purpose of comparison, it follows that the ras peptide resembles the DMPC component, rather than the rigid cholesterol molecules in the liquid-ordered phase. This is despite the increase in the order parameters in the former case (80–82), which is opposite to the ras chains. Another parameter that can be investigated from the experimental data is the value of R_{int}, which is proportional to the correlation time for internal segmental motions of the ras peptide chains. This value can be compared to the extrapolation of the square-law plot to an order parameter $S_{\mathrm{CD}} = 0$, i.e., the intersection with the y axis in Fig. 5. The values of 1.57 and 0.33 determined from the molecular and composite membrane deformation models, respectively, are close to the experimentally determined value of ≈2. As discussed elsewhere (22), this corresponds to a value for the local or microviscosity of the bilayer hydrocarbon core that is similar to that of a light oil such as tetradecane or hexadecane.

Atomistic picture of membrane-bound ras peptide

A previous MD simulation investigated the position, orientation, and flexibility of the membrane-associated ras peptide and confirmed several experimental findings (83). For instance, the lower order of the ras hexadecyl chain in a DMPC matrix, the distribution of the ras lipid chains, backbone, and side chains in the lipid bilayer, and the general model of the ras peptide membrane arrangement could be reproduced. With regard to the interpretation of the relaxation data using MD simulations, the particular advantage is that the order parameters and relaxation rates can be unambiguously assigned to the respective carbon atoms, while the experimental assignments are not exactly known. Therefore, the common analysis of experimental data by analytical as well as MD simulation tools holds promise for improving the understanding of biological problems. Despite the discrepancy in the order parameters, the experimental relaxation rates seem to be relatively well reproduced in the MD simulations. The MD simulations provided a rather exact reproduction of the experimental relaxation rates and their angular dependence. All molecular processes that lead to spin relaxation, with the possible exception of the uppermost chain segments, are well sampled by the MD simulation of 100 ns trajectory (32–34). Although the exact value of the experimental relaxation rates is not always perfectly reproduced, the functional dependence of the angular dependence is very well modeled. In consequence, slower motions

may not contribute very strongly to spin relaxation at the relatively high magnetic field of 17.6 *T*. However, although the relaxation rates are well reproduced in the MD simulation, the square-law plots determined from the simulation deviate appreciably from the experimental data. According to the above discussion, this seems to be caused by the somewhat low simulated order parameters for much of the chain. The sensitive dependence of the order parameter on surface area (45) suggests that a modest adjustment could bring the simulated and experimental order parameter profiles into agreement, quite possibly with little change in relaxation rates. Structural aspects determined from the MD simulation of the membrane-bound ras peptide will be discussed along with $^{13}C/^{15}N$ NMR data in an upcoming study.

In conclusion, this study shows that the C-terminus of the membrane-bound ras protein is highly mobile on the fast timescale. In particular, the lipid modifications that anchor the protein in the membrane undergo large amplitude motions, which would be in agreement with chain backfolding and upturns. This is illustrated in Fig. 8, which represents a snapshot from the MD simulation. We hypothesize that this high mobility of the lipid modifications of ras leads to a further decrease in the free energy of the membrane-bound protein by increasing the configurational entropy. Thus, attachment of the highly flexible protein anchor at the membrane is strong despite the high mobility of the lipid chains, which might run counter to intuition. If a peptide only has a single lipid modification, once a chain upturn is encountered the peptide may diffuse away from the membrane. With the double lipid modification, the likelihood for such an event is much decreased even with the very high chain flexibility. Consequently, a doubly lipid-modified protein may, in part, retain rotational and translational freedom when bound to the membrane because of the high flexibility of the membrane binding segment. Finally, the approach demonstrated here for the ras peptide is also applicable to the entire N-ras protein, where a soluble domain is linked to its membrane anchor. This aspect constitutes an attractive direction for future work focused on the membrane basis for the mechanism of action of human N-ras oncogenes.

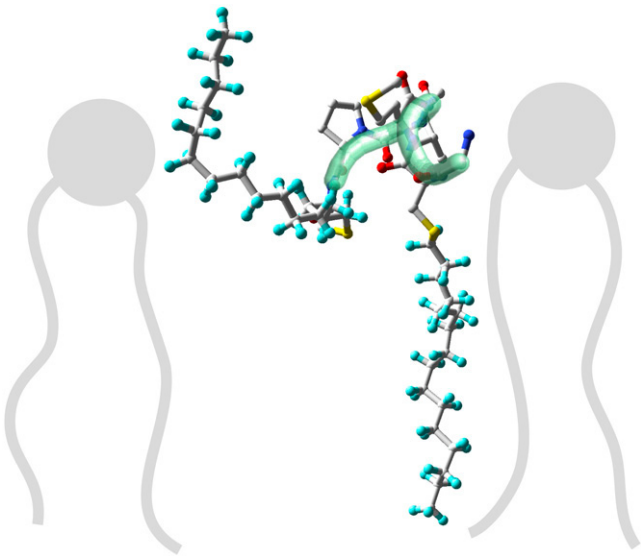

FIGURE 8 Cartoon snapshot derived from molecular dynamics simulations of ras heptapeptide in a DMPC bilayer matrix. Two lipid molecules are schematically drawn.

SUPPLEMENTARY MATERIAL

To view all of the supplemental files associated with this article, visit www.biophysj.org.

The authors thank Dr. Klaus Gawrisch and Prof. Horia Petrache for helpful discussions.

The work was supported by grants from the Deutsche Forschungsgemeinschaft (No. HU 720/5-2 and VO 1523/1-1), U. S. National Institutes of Health (No. EY12049), and U. S. National Science Foundation (Nos. MCB-0543124 and CHE-607917).

REFERENCES

1. Schlesinger, M. J. (editor). 1993. Lipid Modification of Proteins. CRC Press, Boca Raton, FL.
2. Casey, P. J. 1995. Protein lipidation in cell signaling. *Science*. 268: 221–225.
3. Marshall, C. J. 1993. Protein prenylation: a mediator of protein-protein interactions. *Science*. 259:1865–1866.
4. Wittinghofer, A., and H. Waldmann. 2000. Ras—a molecular switch involved in tumor formation. *Angew. Chem. Int. Ed. Engl.* 39:4192–4214.
5. Prior, I. A., and J. F. Hancock. 2001. Compartmentalization of ras proteins. *J. Cell Sci.* 114:1603–1608.
6. Shahinian, S., and J. R. Silvius. 1995. Doubly-lipid-modified protein sequence motifs exhibit long-lived anchorage to lipid bilayer membranes. *Biochemistry*. 34:3813–3822.
7. Pool, C. T., and T. E. Thompson. 1998. Chain length and temperature dependence of the reversible association of model acylated proteins with lipid bilayers. *Biochemistry*. 37:10246–10255.
8. Tanford, C. 1980. The Hydrophobic Effect: Formation of Micelles and Biological Membranes. John Wiley & Sons, New York.
9. Peitzsch, R. M., and S. McLaughlin. 1993. Binding of acylated peptides and fatty acids to phospholipid vesicles: pertinence to myristoylated proteins. *Biochemistry*. 32:10436–10443.
10. Silvius, J. R., and F. l'Heureux. 1994. Fluorimetric evaluation of the affinities of isoprenylated peptides for lipid bilayers. *Biochemistry*. 33: 3014–3022.
11. Huster, D., K. Arnold, and K. Gawrisch. 1999. Investigation of lipid organization in biological membranes by two-dimensional nuclear Overhauser enhancement spectroscopy. *J. Phys. Chem. B*. 103:243–251.
12. Petrache, H. I., N. Gouliaev, S. Tristram-Nagle, R. Zhang, R. M. Suter, and J. F. Nagle. 1998. Interbilayer interactions from high resolution x-ray scattering. *Phys. Rev. E*. 57:7014–7024.
13. Brown, M. F. 1996. Membrane structure and dynamics studied with NMR spectroscopy. *In* Biological Membranes. A Molecular Perspective from Computation and Experiment. K. M. Merz and B. Roux, editors. Birkhäuser, Boston, MA.
14. White, S. H., A. S. Ladokhin, S. Jayasinghe, and K. Hristova. 2001. How membranes shape protein structure. *J. Biol. Chem.* 276:32395–32398.

15. Huster, D., K. Kuhn, D. Kadereit, H. Waldmann, and K. Arnold. 2001. High resolution magic angle spinning NMR for the investigation of a ras lipopeptide in a lipid bilayer. *Angew. Chem. Int. Ed. Engl.* 40: 1056–1058.

16. Huster, D., A. Vogel, C. Katzka, H. A. Scheidt, H. Binder, S. Dante, T. Gutberlet, O. Zschörnig, H. Waldmann, and K. Arnold. 2003. Membrane insertion of a lipidated ras peptide studied by FTIR, solid-state NMR, and neutron diffraction spectroscopy. *J. Am. Chem. Soc.* 125: 4070–4079.

17. Vogel, A., C. P. Katzka, H. Waldmann, K. Arnold, M. F. Brown, and D. Huster. 2005. Lipid modifications of a ras peptide exhibit altered packing and mobility versus host membrane as detected by ^{2}H solid-state NMR. *J. Am. Chem. Soc.* 127:12263–12272.

18. Reuther, G., K.-T. Tan, J. Köhler, C. Nowak, A. Pampel, K. Arnold, J. Kuhlmann, H. Waldmann, and D. Huster. 2006. Structural model of the membrane-bound C-terminus of lipid-modified human N-ras protein. *Angew. Chem. Int. Ed. Engl.* 45:5387–5390.

19. Reuther, G., K.-T. Tan, A. Vogel, C. Nowak, J. Kuhlmann, H. Waldmann, and D. Huster. 2006. The lipidated membrane anchor of the N-ras protein shows an extensive dynamics as revealed by solid-state NMR. *J. Am. Chem. Soc.* 128:13840–13846.

20. Müller, K., P. Meier, and G. Kothe. 1985. Multipulse dynamic NMR of liquid crystal polymers. *Prog. Nucl. Magn. Reson. Spectrosc.* 17:211–239.

21. Vold, R. R., and R. L. Vold. 1991. Deuterium relaxation in molecular solids. *In* Advances in Magnetic and Optical Resonance. W. S. Warren, editor. Academic Press, San Diego, CA.

22. Brown, M. F. 1982. Theory of spin-lattice relaxation in lipid bilayers and biological membranes. ^{2}H and ^{14}N quadrupolar relaxation. *J. Chem. Phys.* 77:1576–1799.

23. Pastor, R. W., R. M. Venable, and S. E. Feller. 2002. Lipid bilayers, NMR relaxation, and computer simulations. *Acc. Chem. Res.* 35:438–446.

24. Trouard, T. P., A. A. Nevzorov, T. M. Alam, C. Job, J. Zajicek, and M. F. Brown. 1999. Influence of cholesterol on dynamics of dimyristoylphosphatidylcholine bilayers as studied by deuterium NMR relaxation. *J. Chem. Phys.* 110:8802–8818.

25. Nevzorov, A. A., T. P. Trouard, and M. F. Brown. 1998. Lipid bilayer dynamics from simultaneous analysis of orientation and frequency dependence of deuterium spin-lattice and quadrupolar order relaxation. *Phys. Rev. E.* 58:2259–2281.

26. Nevzorov, A. A., and M. F. Brown. 1997. Dynamics of lipid bilayers from comparative analysis of ^{2}H and ^{13}C nuclear magnetic resonance relaxation data as a function of frequency and temperature. *J. Chem. Phys.* 107:10288–10310.

27. Trouard, T. P., T. M. Alam, and M. F. Brown. 1994. Angular dependence of deuterium spin-lattice relaxation rates of macroscopically oriented dilauroylphosphatidylcholine in the liquid-crystalline state. *J. Chem. Phys.* 101:5229–5261.

28. Prosser, R. S., and J. H. Davis. 1994. Dynamics of an integral membrane peptide: a deuterium NMR relaxation study of gramicidin. *Biophys. J.* 66:1429–1440.

29. Karplus, M. 2002. Molecular dynamics simulations of biomolecules. *Acc. Chem. Res.* 35:321–323.

30. Huber, T., K. Rajamoorthi, V. F. Kurze, K. Beyer, and M. F. Brown. 2002. Structure of docosahexaenoic acid-containing phospholipid bilayers as studied by ^{2}H NMR and molecular dynamics simulations. *J. Am. Chem. Soc.* 124:298–309.

31. Leekumjorn, S., and A. K. Sum. 2006. Molecular simulation study of structural and dynamic properties of mixed DPPC/DPPE bilayers. *Biophys. J.* 90:3951–3965.

32. Feller, S. E., K. Gawrisch, and A. D. MacKerell, Jr. 2002. Polyunsaturated fatty acids in lipid bilayers: intrinsic and environmental contributions to their unique physical properties. *J. Am. Chem. Soc.* 124: 318–326.

33. Eldho, N. V., S. E. Feller, S. Tristram-Nagle, I. V. Polozov, and K. Gawrisch. 2003. Polyunsaturated docosahexaenoic vs. docosapentaenoic acid-differences in lipid matrix properties from the loss of one double bond. *J. Am. Chem. Soc.* 125:6409–6421.

34. Lindahl, E., and O. Edholm. 2001. Molecular dynamics simulation of NMR relaxation rates and slow dynamics in lipid bilayers. *J. Chem. Phys.* 115:4938–4950.

35. Feller, S. E., D. Huster, and K. Gawrisch. 1999. Interpretation of NOESY cross-relaxation rates from molecular dynamics simulations of a lipid bilayer. *J. Am. Chem. Soc.* 121:8963–8964.

36. Feller, S. E., C. A. Brown, D. T. Nizza, and K. Gawrisch. 2002. Nuclear Overhauser enhancement spectroscopy cross-relaxation rates and ethanol distribution across membranes. *Biophys. J.* 82:1396–1404.

37. Feller, S. E., K. Gawrisch, and T. B. Woolf. 2003. Rhodopsin exhibits a preference for solvation by polyunsaturated docosohexaenoic acid. *J. Am. Chem. Soc.* 125:4434–4435.

38. Grossfield, A., S. E. Feller, and M. C. Pitman. 2006. A role for direct interactions in the modulation of rhodopsin by ω3 polyunsaturated lipids. *Proc. Natl. Acad. Sci. USA.* 103:4888–4893.

39. Crozier, P. S., M. J. Stevens, L. R. Forrest, and T. B. Woolf. 2003. Molecular dynamics simulation of dark-adapted rhodopsin in an explicit membrane bilayer: coupling between local retinal and larger scale conformational change. *J. Mol. Biol.* 333:493–514.

40. Huber, T., A. V. Botelho, K. Beyer, and M. F. Brown. 2004. Membrane model for the G-protein-coupled receptor rhodopsin: hydrophobic interface and dynamical structure. *Biophys. J.* 86:2078–2100.

41. Hinterding, K., D. Alonso-Diaz, and H. Waldmann. 1998. Organic synthesis and biological signal transduction. *Angew. Chem. Int. Ed. Engl.* 37:688–749.

42. Nägele, E., M. Schelhaas, N. Kuder, and H. Waldmann. 1998. Chemoenzymatic synthesis of N-ras lipopeptides. *J. Am. Chem. Soc.* 120: 6889–6902.

43. Schelhaas, M., S. Glomsda, M. Hänsler, H.-D. Jakubke, and H. Waldmann. 1996. Enzymatic synthesis of peptides and ras lipopeptides employing choline ester as a solubilizing, protecting, and activating group. *Angew. Chem. Int. Ed. Engl.* 35:106–109.

44. Davis, J. H., K. R. Jeffrey, M. Bloom, M. I. Valic, and T. P. Higgs. 1976. Quadrupolar echo deuteron magnetic resonance spectroscopy in ordered hydrocarbon chains. *Chem. Phys. Lett.* 42:390–394.

45. Petrache, H. I., S. W. Dodd, and M. F. Brown. 2000. Area per lipid and acyl length distributions in fluid phosphatidylcholines determined by ^{2}H NMR spectroscopy. *Biophys. J.* 79:3172–3192.

46. Brooks, B. R., R. E. Bruccoleri, B. D. Olafson, D. J. States, S. Swaminathan, and M. Karplus. 1983. CHARMM—a program for macromolecular energy, minimization, and dynamics calculations. *J. Comput. Chem.* 4:187–217.

47. MacKerell, A. D., D. Bashford, M. Bellott, R. L. Dunbrack, J. D. Evanseck, M. J. Field, S. Fischer, J. Gao, H. Guo, S. Ha, D. Joseph-McCarthy, L. Kuchnir, K. Kuczera, F. T. K. Lau, C. Mattos, S. Michnick, T. Ngo, D. T. Nguyen, B. Prodhom, W. E. Reiher, B. Roux, M. Schlenkrich, J. C. Smith, R. Stote, J. Straub, M. Watanabe, J. Wiorkiewicz-Kuczera, D. Yin, and M. Karplus. 1998. All-atom empirical potential for molecular modeling and dynamics studies of proteins. *J. Phys. Chem. B.* 102:3586–3616.

48. Klauda, J. B., B. R. Brooks, A. D. MacKerell, R. M. Venable, and R. W. Pastor. 2005. An ab initio study on the torsional surface of alkanes and its effect on molecular simulations of alkanes and a DPPC bilayer. *J. Phys. Chem. B.* 109:5300–5311.

49. Essmann, U., L. Perera, M. L. Berkowitz, T. Darden, H. Lee, and L. G. Pedersen. 1995. A smooth particle mesh Ewald method. *J. Chem. Phys.* 103:8577–8593.

50. van Gunsteren, W., and H. J. C. Berendsen. 1977. Algorithms for macromolecular dynamics and constraint dynamics. *Mol. Phys.* 34: 1311–1327.

51. Torchia, D. A., and A. Szabo. 1982. Spin-lattice relaxation in solids. *J. Magn. Reson.* 49:107–121.

52. Nevzorov, A. A., T. P. Trouard, and M. F. Brown. 1997. Correlation functions for lipid membrane dynamics obtained from NMR spectroscopy. *Phys. Rev. E.* 55:3276–3282.

53. Vold, R. R. 1994. Deuterium NMR studies of dynamics in solids and liquid crystals. *In* Nuclear Magnetic Resonance Probes of Molecular Dynamics. R. Tycko, Editor. Kluwer Academic Publishers, Dordrecht, The Netherlands.

54. Schindler, H., and J. Seelig. 1975. Deuterium order parameters in relation to thermodynamic properties of a phospholipid bilayer. A statistical mechanical interpretation. *Biochemistry.* 14:2283–2287.

55. Petrache, H. I., A. Salmon, and M. F. Brown. 2001. Structural properties of docosahexaenoyl phospholipid bilayers investigated by solid-state ^{2}H NMR spectroscopy. *J. Am. Chem. Soc.* 123:12611–12622.

56. Holte, L. L., S. A. Peter, T. M. Sinnwell, and K. Gawrisch. 1995. ^{2}H nuclear magnetic resonance order parameter profiles suggest a change of molecular shape for phosphatidylcholines containing a polyunsaturated acyl chain. *Biophys. J.* 68:2396–2403.

57. Gawrisch, K., N. V. Eldho, and L. L. Holte. 2003. The structure of DHA in phospholipid membranes. *Lipids.* 38:445–452.

58. Feller, S. E., and K. Gawrisch. 2005. Properties of docosahexaenoic-acid-containing lipids and their influence on the function of rhodopsin. *Curr. Opin. Struct. Biol.* 15:416–422.

59. Rajamoorthi, K., H. I. Petrache, T. J. McIntosh, and M. F. Brown. 2005. Packing and viscoelasticity of polyunsaturated ω-3 and ω-6 lipid bilayers as seen by ^{2}H NMR and x-ray diffraction. *J. Am. Chem. Soc.* 127:1576–1588.

60. Otten, D., M. F. Brown, and K. Beyer. 2000. Softening of membrane bilayers by detergents elucidated by deuterium NMR spectroscopy. *J. Phys. Chem. B.* 104:12119–12129.

61. Bonmatin, J. M., I. C. Smith, H. C. Jarrell, and D. J. Siminovitch. 1990. Use of a comprehensive approach to molecular dynamics in ordered lipid systems—cholesterol reorientation in oriented lipid bilayers. A ^{2}H NMR relaxation study. *J. Am. Chem. Soc.* 112:1697–1704.

62. Mayer, C., G. Gröbner, K. Müller, K. Weisz, and G. Kothe. 1990. Orientation-dependent deuteron spin-lattice relaxation times in bilayer membranes: characterization of the overall lipid motion. *Chem. Phys. Lett.* 165:155–161.

63. Siminovitch, D. J. 1998. Solid-state NMR studies of proteins: the view from static ^{2}H NMR experiments. *Biochem. Cell Biol.* 76: 411–422.

64. Watts, A. 2005. Solid-state NMR in drug design and discovery for membrane-embedded targets. *Nat. Rev. Drug Discov.* 4:555–568.

65. Davis, J. H., and M. Auger. 1999. Static and magic angle spinning NMR of membrane peptides and proteins. *Prog. Nucl. Magn. Reson. Spectrosc.* 35:1–84.

66. Gumbart, J., Y. Wang, A. Aksimentiev, E. Tajkhorshid, and K. Schulten. 2005. Molecular dynamics simulations of proteins in lipid bilayers. *Curr. Opin. Struct. Biol.* 15:423–431.

67. Ash, W. L., M. R. Zlomislic, E. O. Oloo, and D. P. Tieleman. 2004. Computer simulations of membrane proteins. *Biochim. Biophys. Acta.* 1666:158–189.

68. Roux, B. 2002. Computational studies of the gramicidin channel. *Acc. Chem. Res.* 35:366–375.

69. Feller, S. E., and K. Gawrisch. 2005. Properties of docosahexaenoic-acid-containing lipids and their influence on the function of rhodopsin. *Curr. Opin. Struct. Biol.* 15:416–422.

70. Gumbart, J., Y. Wang, A. Aksimentiev, E. Tajkhorshid, and K. Schulten. 2005. Molecular dynamics simulations of proteins in lipid bilayers. *Curr. Opin. Struct. Biol.* 15:423–431.

71. Ash, W. L., M. R. Zlomislic, E. O. Oloo, and D. P. Tieleman. 2004. Computer simulations of membrane proteins. *Biochim. Biophys. Acta.* 1666:158–189.

72. Efremov, R. G., D. E. Nolde, A. G. Konshina, N. P. Syrtcev, and A. S. Arseniev. 2004. Peptides and proteins in membranes: what can we learn via computer simulations? *Curr. Med. Chem.* 11:2421–2442.

73. Feller, S. E., and K. Gawrisch. 2005. Properties of docosahexaenoic-acid-containing lipids and their influence on the function of rhodopsin. *Curr. Opin. Struct. Biol.* 15:416–422.

74. Salmon, A., S. W. Dodd, G. D. Williams, J. M. Beach, and M. F. Brown. 1987. Configurational statistics of acyl chains in polyunsaturated lipid bilayers from deuterium NMR. *J. Am. Chem. Soc.* 109:2600–2609.

75. Bloom, M., and E. Evans. 1991. Observation of surface undulations on the mesoscopic length scale by NMR. *In* Biologically Inspired Physics. L. Peliti, editor. Plenum Press, New York.

76. Huster, D. 2005. Investigations of the structure and dynamics of membrane-associated peptides by magic angle spinning NMR. *Prog. Nucl. Magn. Reson. Spectrosc.* 46:79–107.

77. Ketchem, R. R., W. Hu, and T. A. Cross. 1993. High-resolution conformation of gramicidin A in a lipid bilayer by solid-state NMR. *Science.* 261:1457–1460.

78. Brown, M. F. 1990. Anisotropic nuclear-spin relaxation of cholesterol in phospholipid bilayers. *Mol. Phys.* 71:903–908.

79. Trouard, T. P., T. M. Alam, J. Zajicek, and M. F. Brown. 1992. Angular anisotropy of ^{2}H NMR spectral densities in phospholipid-bilayers containing cholesterol. *Chem. Phys. Lett.* 189:67–75.

80. Brown, M. F., R. L. Thurmond, S. W. Dodd, D. Otten, and K. Beyer. 2001. Composite membrane deformation on the mesoscopic length scale. *Phys. Rev. E.* 64:010901.

81. Martinez, G. V., E. M. Dykstra, S. Lope-Piedrafita, C. Job, and M. F. Brown. 2002. NMR elastometry of fluid membranes in the mesoscopic regime. *Phys. Rev. E.* 66:050902.

82. Martinez, G. V., E. M. Dykstra, S. Lope-Piedrafita, and M. F. Brown. 2004. Lanosterol and cholesterol-induced variations in bilayer elasticity probed by ^{2}H NMR relaxation. *Langmuir.* 20:1043–1046.

83. Gorfe, A. A., R. Pellarin, and A. Caflisch. 2004. Membrane localization and flexibility of a lipidated ras peptide studied by molecular dynamics simulations. *J. Am. Chem. Soc.* 126:15277–15286.